applied optics

Polarization property analysis of a periscopic scanner with three-dimensional polarization ray-tracing calculus

YUFEI YANG[1,2,*] AND CHANGXIANG YAN[1]

[1]Changchun Institute of Optics, Fine Mechanics and Physics, Chinese Academy of Science, Changchun 130033, China
[2]University of Chinese Academy of Sciences, Beijing 100049, China
*Corresponding author: yangyufei0904@163.com

Received 9 November 2015; revised 11 January 2016; accepted 11 January 2016; posted 11 January 2016 (Doc. ID 252538); published 19 February 2016

The polarization properties of a two-axis periscopic optical scanner constituted by a pair of rotating planar mirrors have been studied by using the three-dimensional polarization ray-tracing matrix method. The separate and cumulative matrices that define the transformation of the polarization state are obtained and expressed in terms of the rotation angles of two mirrors. The variations of diattenuation and retardance are investigated and graphically shown as functions of the rotation angles. On this basis, a further investigation about the cumulative polarization aberrations of three different metal-coated periscopic scanners is accomplished. Finally, the output polarization states of the three metal-coated scanners are calculated with the input beam of the arbitrary polarization states, and the results show that aluminum film is more appropriate than gold film or silver film for the polarization-maintaining periscopic scanner.

OCIS codes: (260.5430) Polarization; (080.1010) Aberrations (global); (080.0080) Geometric optics; (120.2130) Ellipsometry and polarimetry; (060.1660) Coherent communications.

http://dx.doi.org/10.1364/AO.55.001343

1. INTRODUCTION

A periscopic scanner is a device constituted by two rotating planar mirrors that are used to deflect a laser beam along the global sphere system. Unlike the galvanometric scanner, which deflects the beam along two perpendicular directions, the periscopic scanner mounted on laser communication terminals allows us to point and track the directions across a full hemisphere [1]. For the periscopic scanner, the optical system is intended to maintain the input polarization states, yet the optical interfaces cause some polarization changes to the light at nonnormal incidence. The polarization changes are referred to as instrumental polarization. Mirrors with thin-film coatings induce polarization variations, in both diattenuation and retardance, as a function of the incident angle [2–4]. For a periscopic scanner, the diattenuation and retardance of the two mirrors change the polarization state of the input beam. The variations in the polarization states significantly affect the signal demodulated in the receiving terminals; they are first-order effects, especially occurring in optical communication systems utilizing local oscillators for heterodyne detection [2]. Therefore, in this kind of application, it is of primary importance to understand how the polarization state of the output beam changes as a function of the combined motion of the mirrors.

Previous studies of the changes in the polarization state caused by reflections of a light beam upon moving mirrors refer to optical configurations quite different from that of a periscopic scanner, such as sky scanners [5], coelostats [6], and the galvanometric scanner [7,8]. For the periscopic scanner, a simple model is presented and used to explain the three-dimensional generalization of the Jones calculus in references [9,10]. A similar model is presented in [11] to describe the balancing of polarization aberrations. These three references are mainly aimed at studying the theory of three-dimensional polarization ray-tracing calculus, yet a detailed and complete analysis of the rotating periscopic scanner is not particularly performed. For this reason, the principal purpose of the present work is to give a theoretical description of the polarization aberrations caused by the motion of the two mirrors of a periscopic scanner.

In this paper, the polarization properties of the periscopic scanner are studied based on the three-dimensional polarization ray-tracing algorithm. A further investigation of polarization aberrations is performed for three different metal-coated scanners. Comparing these three metallic coatings, the polarization-maintaining capacity of the periscopic scanner is analyzed.

This paper is structured as follows. Section 2 describes the optical configuration of a periscopic scanner and calculates the

matrix that gives the propagation direction of the output beam. Section 3 introduces the algorithm of three-dimensional polarization ray tracing. Section 4 investigates the polarization aberrations of a periscopic scanner. In order to give a better description of the polarization aberrations, the diattenuation and retardance of several scan angles are calculated and graphically plotted. Section 5 compares the polarization aberrations of three different metal-coated periscopic scanners and further investigates the polarization states of the output beam when the input beam is of arbitrary polarization. Section 6 gives the concluding remarks.

2. GEOMETRY OF THE PERISCOPIC SCANNER

A periscopic scanner controls the direction of the output beam by rotating the two mirrors about the corresponding rotation axes. The two perpendicular rotation axes are named rotation axis 1 and rotation axis 2. The two axes remain perpendicular to each other. Mirrors 1 (M1) and 2 (M2) are perfectly flat, with no deformation occurring while rotating. The antenna and mirror M1 are connected by a metal cylinder C1 with rotation axis 1 attached on the cylinder. Mirrors M1 and M2 are connected by a metal cylinder C2 with rotation axis 2 attached on it. Rotation axis 1 controls the rotation of the combined parts, including M1, M2, C1, and C2. The rotation of axis 2 only controls the rotation of mirror M2. To simplify ray tracing, the periscopic scanner is shown in Fig. 1. Given a right-handed global coordinate system O(x, y, z), there are two local coordinate systems depicted in Fig. 1. The local coordinate system O1($x1, y1, z1$) is right-handed, while the local coordinate system O2($x2, y2, z2$) is left-handed. The aligned errors between mirrors and rotation axes are neglected. Therefore, the polarization aberrations induced by the static and dynamic rotation errors are omitted in this paper. Mirror M1 sweeps the reflected beam in the local $x1$–$y1$ plane, while mirror M2 sweeps the directions of the output beam in the local $x2$–$y2$ plane. Both rotations are compared to a predefined "zero position." The zero position is achieved in the global coordinate system when the vector normal to the reflective surface of M1 is $[0, \sqrt{2}/2, \sqrt{2}/2]$ and the vector normal to the surface of M2 is $[0, -\sqrt{2}/2, -\sqrt{2}/2]$. The surface normal of the interface is defined as pointing toward the transmitted medium, which is shown in Fig. 1. The input parallel beam initially propagates along the positive z axis, and the wave vector is $\mathbf{k}_{in} = [0, 0, 1]$. When the mirrors are at the zero positions, the output beam will come out along the positive z axis with $\mathbf{k}_{out} = [0, 0, 1]$.

In order to find the zero positions of the mirrors, we introduce the criterion to describe rotations that will be used throughout the paper. The rotation of axis 1 is right-handed about the global positive z axis, and the angle is referred to as the azimuth angle α. The rotation of axis 2 is left-handed about the local positive $z2$ axis, and the corresponding angle is referred to as the elevation angle β. The rotation of axis 1 changes the local coordinate system O2, but the rotation of axis 2 continues rotating about the local $z2$ axis. According to this criterion, the zero position of M1 and M2 corresponds to $\alpha = \beta = 0°$. When the scanner is at the rotation angles ($\alpha = 0°$, $\beta = 90°$), the output beam vector is $\mathbf{k}_{out} = [1, 0, 0]$ and the corresponding direction is the positive x axis in the global coordinate system.

The direction vector of the output beam is derived from the azimuth angle α and elevation angle β. Starting from the zero position, the normal to the surface of M1 is associated with azimuth angle α and is generally defined by

$$\mathbf{n}_{M1} = \frac{1}{\sqrt{2}} \begin{bmatrix} -\sin\alpha \\ \cos\alpha \\ 1 \end{bmatrix}. \tag{1}$$

The rotation of M2 is related to the order of rotation. We assume the first rotation is axis 1 and the second rotation is axis 2; hence, the normal to the surface of M2 is expressed as

$$\mathbf{n}_{M2} = -\frac{1}{\sqrt{2}} \begin{bmatrix} -\sin\alpha + \cos\alpha \sin\beta \\ \cos\alpha + \sin\alpha \sin\beta \\ \cos\beta \end{bmatrix}. \tag{2}$$

The reflection of a ray upon a mirror whose normal has components $\mathbf{n} = [n_x, n_y, n_z]$ is generally described by the matrix

$$\mathbf{H} = \begin{bmatrix} 1 - 2n_x^2 & -2n_x n_y & -2n_x n_z \\ -2n_x n_y & 1 - 2n_y^2 & -2n_y n_z \\ -2n_x n_z & -2n_y n_z & 1 - 2n_z^2 \end{bmatrix}. \tag{3}$$

Therefore, the reflection matrix associated with M1 is obtained by using the components of the normal vector shown in Eq. (1):

$$\mathbf{H}_1 = \begin{bmatrix} 1 - \sin^2\alpha & \sin\alpha\cos\alpha & \sin\alpha \\ \sin\alpha\cos\alpha & 1 - \cos^2\alpha & -\cos\alpha \\ \sin\alpha & -\cos\alpha & 0 \end{bmatrix}. \tag{4}$$

Similarly, the reflection matrix of M2 is obtained by using the same method:

$$\mathbf{H}_2 = \begin{bmatrix} 1 - (\sin\alpha - \cos\alpha\sin\beta)^2 & (\cos\alpha + \sin\alpha\sin\beta)(\sin\alpha - \cos\alpha\sin\beta) & \cos\beta(\sin\alpha - \cos\alpha\sin\beta) \\ (\cos\alpha + \sin\alpha\sin\beta)(\sin\alpha - \cos\alpha\sin\beta) & 1 - (\cos\alpha + \sin\alpha\sin\beta)^2 & -\cos\beta(\cos\alpha + \sin\alpha\sin\beta) \\ \cos\beta(\sin\alpha - \cos\alpha\sin\beta) & -\cos\beta(\cos\alpha + \sin\alpha\sin\beta) & 1 - \cos^2\beta \end{bmatrix}. \tag{5}$$

The transformation matrix of the periscopic scanning system, i.e., the matrix $\mathbf{H}$, is finally given by the matrix product between the reflection matrices of the two mirrors. Since any ray of the input beam is first reflected by M1 and then by M2, the H matrix is given by $\mathbf{H} = \mathbf{H}_2\mathbf{H}_1$.

The input collimated beam initially propagates along the positive z axis, and the wave vector is $\mathbf{k}_{in} = [0, 0, 1]$. After the reflection of M1, the ray vector is

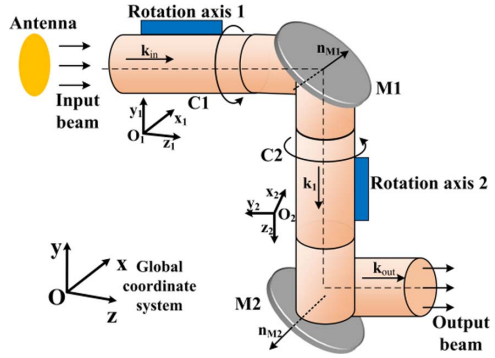

Fig. 1. Schematic view of the periscopic scanning system considered in this paper, together with the global coordinate system O and two local coordinate systems O1 and O2. The surface normal vectors **n** and wave vectors **k** used in the calculations are shown.

$$\mathbf{k}_1 = \begin{bmatrix} \sin\alpha \\ -\cos\alpha \\ 0 \end{bmatrix}. \tag{6}$$

The final propagation vector will be

$$\mathbf{k}_{\text{out}} = \begin{bmatrix} \cos\alpha \sin\beta \\ \sin\alpha \sin\beta \\ \cos\beta \end{bmatrix}. \tag{7}$$

3. THREE-DIMENSIONAL POLARIZATION RAY TRACING

In this section, we will introduce and perform the three-dimensional polarization ray-tracing algorithm. According to the beam propagation vector **k** and surface normal vector **n**, the polarization aberrations can be performed with the Jones matrices in three dimensions for a planar wavefront [9]. The Jones vector specially refers to a monochromatic plane wave describing the electric field and the polarization ellipse with respect to a local coordinate system associated with the particular transverse plane [11]. In three-dimensional polarization ray tracing, the electric field and polarization ellipse are expressed in the global coordinate system.

The three-dimensional polarization ray-tracing algorithm has been presented by Yun *et al.* [9,10]. Polarization effects are propagated along ray paths through optical systems by multiplication of **P** matrices for each ray interception. The **P** matrix at each interaction is expressed by a three-by-three matrix that is associated with the incident angle and medium at each surface [9]. Upon reflection from mirrors, there is a reflected electric field difference in amplitude and phase between *s*- and *p*-polarized light. The orientation of the *s*- and *p*-polarized components is a function of the light propagation direction **k** and the surface normal vector **n**:

$$s_q = \frac{k_{q-1} \times k_q}{|k_{q-1} \times k_q|}, \qquad p_q = k_{q-1} \times s_q,$$
$$s'_q = s_q, \qquad p'_q = k_q \times s_q. \tag{8}$$

The index q represents the number of mirrors. According to this definition, the *s*- and *p*-polarized components of reflection mirror M1 are expressed as

$$s_1 = s'_1 = [\cos\alpha \quad \sin\alpha \quad 0]^T,$$
$$p_1 = [-\sin\alpha \quad \cos\alpha \quad 0]^T,$$
$$p'_1 = [0 \quad 0 \quad 1]^T. \tag{9}$$

Similarly, the *s*- and *p*-polarized components of M2 are

$$s_2 = s'_2 = [-\cos\alpha\cos\beta \quad -\cos\beta\sin\alpha \quad \sin\beta]^T,$$
$$p_2 = [-\cos\alpha\sin\beta \quad -\sin\alpha\sin\beta \quad -\cos\beta]^T,$$
$$p'_2 = [\sin\alpha \quad -\cos\alpha \quad 0]^T. \tag{10}$$

The **P** matrix is obtained using the equation below, and a detailed demonstration is presented in Ref. [9]:

$$\mathbf{P}_q = \begin{pmatrix} s_{x,q} & p'_{x,q} & k_{x,q} \\ s_{y,q} & p'_{y,q} & k_{y,q} \\ s_{z,q} & p'_{z,q} & k_{z,q} \end{pmatrix} \quad \mathbf{J}_q \begin{pmatrix} s_{x,q} & s_{y,q} & s_{z,q} \\ p_{x,q} & p_{y,q} & p_{z,q} \\ k_{x,q-1} & k_{y,q-1} & k_{z,q-1} \end{pmatrix}. \tag{11}$$

The matrix $\mathbf{J}_q$ is the three-dimensional Jones matrix and is given by

$$\mathbf{J}_q = \begin{bmatrix} r_{s,q} & 0 & 0 \\ 0 & r_{p,q} & 0 \\ 0 & 0 & 1 \end{bmatrix}. \tag{12}$$

$r_{s,q}$ and $r_{p,q}$ are the Fresnel reflection coefficients for *s*- and *p*-polarized light, respectively, reflected from a mirror or the corresponding coefficients calculated for a thin-film-coated interface [12]. Therefore, the polarization matrices of mirrors M1 and M2 can be expressed as

$$\mathbf{P}_1 = \begin{bmatrix} r_s\cos^2\alpha & r_s\cos\alpha\sin\alpha & \sin\alpha \\ r_s\cos\alpha\sin\alpha & r_s\sin^2\alpha & -\cos\alpha \\ -r_p\sin\alpha & r_p\cos\alpha & 0 \end{bmatrix}, \tag{13}$$

$$\mathbf{P}_2 = \begin{bmatrix} r_s\cos^2\alpha\cos^2\beta + \cos\alpha\sin\alpha\sin\beta - r_p\cos\alpha\sin\alpha\sin\beta & -\sin\beta\cos^2\alpha + r_s\cos\alpha\sin\alpha\cos^2\beta - r_p\sin\beta\sin^2\alpha & -r_p\cos\beta\sin\alpha - r_s\cos\alpha\cos\beta\sin\beta \\ r_p\sin\beta\cos^2\alpha + r_s\cos\alpha\sin\alpha\cos^2\beta + \sin\beta\sin^2\alpha & r_s\cos^2\beta\sin^2\alpha - \cos\alpha\sin\alpha\sin\beta + r_p\cos\alpha\sin\alpha\sin\beta & r_p\cos\alpha\cos\beta - r_s\cos\beta\sin\alpha\sin\beta \\ \cos\beta\sin\alpha - r_s\cos\alpha\sin\beta\cos\beta & -\cos\alpha\cos\beta - r_s\cos\beta\sin\alpha\sin\beta & r_s\sin^2\beta \end{bmatrix}. \tag{14}$$

The polarization transformation matrix of a periscopic scanner $\mathbf{P}_{\text{total}}$ is the multiplication of $\mathbf{P}_1$ and $\mathbf{P}_2$; in addition, the polarization state of the output beam is calculated by the matrix multiplication of $\mathbf{P}_{\text{total}}$ and $\mathbf{E}_{\text{in}}$:

$$\mathbf{P}_{\text{total}} = \mathbf{P}_2\mathbf{P}_1,$$
$$\mathbf{E}_{\text{out}} = \mathbf{P}_{\text{total}}\mathbf{E}_{\text{in}}. \tag{15}$$

Polarization elements such as polarizers, retarders, and depolarizers have three general polarization properties: diattenuation, retardance, and depolarization [13]. Diattenuation describes the magnitude of the variation of the transmitted irradiance as a function of the incident polarization state. Retardance is the phase change a device introduces between its eigenpolarizations (eigenstates). Depolarization is intrinsically associated with scattering and a loss of coherence in the polarization state. It involves partially polarized light, and is hard to handle by Jones calculus. In this paper, the absorption of films and materials and the depolarization are ignored. We only analyze the diattenuation and retardance induced by the periscopic scanner. The diattenuation is achieved via the singular value decomposition of the **P** matrix, and is calculated by the eigenvalues of the two eigenpolarizations [9]. The retardance is calculated by removing the geometric transformation from the **P** matrix; the detailed algorithm is listed in [10,11].

4. POLARIZATION PROPERTIES OF THE PERISCOPIC SCANNER

In this section, the gold-coated periscopic scanner is created and the separate and cumulative diattenuation and retardance of the two mirrors are analyzed. Assuming that the operating wavelength of the periscopic scanner is 1550 nm, the complex amplitude reflection coefficients for gold at 1550 nm with refractive index $0.5591 + 9.8112i$ [14,15] are plotted in Fig. 2 as a function of the incident angle. At normal incidence ($i = 0°$), *s*-polarized light and *p*-polarized light are degenerate, so their amplitude and phase change upon reflection are identical, and the diattenuation and retardance are zero.

The incident parallel rays maintain a 45° angle of incidence at the two mirrors when the mirrors rotate about the two axes. The complex amplitude reflection coefficients for gold at 1550 nm are $r_s = 0.9946\,e^{2.9897i}$, $r_p = 0.9891\,e^{-0.3037i}$. Since the two mirrors are made of the same material, by substituting r_s and r_p into Eqs. (13)–(15), the polarization transformation matrices $\mathbf{P}_1$, $\mathbf{P}_2$, and $\mathbf{P}_{\text{total}}$ become functions of azimuth angle α and elevation angle β. The polarization matrix **P** varies with the change of rotation angle and results in the variations in amplitude and orientation of diattenuation and retardance. Moreover, the rotation also changes the polarization state of the output beam.

To evaluate the polarization aberrations of the two mirrors, we choose six groups of rotation angles (α, β) and perform the polarization ray tracings. The surface normal vectors, the output vectors, and the polarization ray-tracing matrices are calculated and listed in Table 1. The units for rotation angle and retardance are degrees.

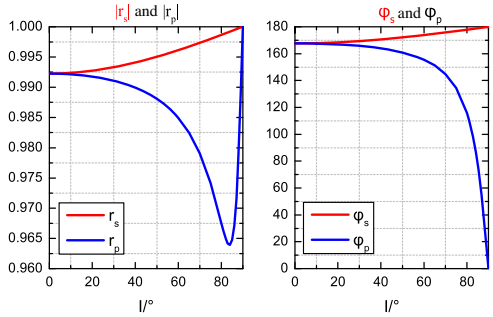

Fig. 2. Fresnel reflection coefficients: amplitude (left) and phase (right) as a function of the incident angle for an air/gold interface at 1550 nm. Red is for *s*-polarized light, and blue is for *p*-polarized light.

The singular value decomposition of the **P** matrix is performed about the six groups of rotation angles. In order to illustrate the dynamic variations of diattenuation and retardance, we calculate the polarization aberrations of M1 and M2 and list them in Tables 2 and 3. The separate and cumulative diattenuation and retardance are tabulated in Tables 2 and 3. The circular diattenuation and circular retardance are taken into account [13,16], and the corresponding orientation θ and ellipticity ε of the diattenuation and retardance are calculated and listed in Tables 2 and 3.

Tables 2 and 3 indicate that the magnitudes of diattenuation and retardance of mirrors M1 and M2 are unchanged, yet the cumulative magnitudes vary with the rotation of the two mirrors. In order to graphically show the dynamic variations in the polarization aberrations, we introduce the plots of the line segments indicating the magnitudes and orientations of diattenuation and retardance. The length of each line segment on the map represents the magnitude of the diattenuation and retardance. The orientation of a line indicates the orientation of the corresponding parameter. The orientation of diattenuation corresponds to the orientation of the polarization state with the maximum transmission. In the metal reflection shown in Fig. 2, the *s*-polarized light has a higher reflection than *p*-polarized light, so the orientation of reflection diattenuation is along the *s*-polarization state. The orientation of retardance corresponds to the polarization state with the smaller phase shift. In Fig. 2, the *p*-polarized light has a smaller phase delay than *s*-polarized light, so the orientation of retardance is along the *p*-polarization state.

The incident parallel beams are simulated by a grid of rays evenly sampling the planar wavefront [11]. To visualize these rotations of polarization properties, the polarization aberrations are projected into the entrance pupil. The diattenuations for the two-mirror systems are shown in Fig. 3. The diattenuations of M1 and M2 are shown in the top two rows of Fig. 3. The cumulative diattenuations of the combination of M1 and M2 are shown in the bottom row of Fig. 3. Figure 4 contains the corresponding retardance maps. According to the definition, the line segments plotted in Fig. 3 are the projections of *s*-polarized light into the entrance pupil. Similarly, the line segments plotted in Fig. 4 are the projections of *p*-polarized light. Therefore, the orientations of cumulative diattenuation and cumulative retardance shown in Figs. 3 and 4 are approximately orthogonal to each other. All the diattenuation and retardance axes shown are viewed from the entrance pupil, so all the maps are compared directly in the same pupil.

The cumulative diattenuation and cumulative retardance are the vector sums of two separate instances of diattenuation and retardance. According to the former four groups in Fig. 3, when the elevation angle β is fixed, the rotations of azimuth angle α change the orientations of diattenuation and keep the magnitudes constant. Comparing these six groups of plots in Fig. 3, the rotations of elevation angle β not only change the magnitudes, but also change the orientations of diattenuation. When $\beta = 0°$, the orientations of diattenuation of M1 and M2 are

Table 1. Surface Normal Vectors, Output Vectors, and Polarization Ray-Tracing Matrices Associated with a Ray Path through a Gold-Coated Periscopic Scanner

Scan Angle (α, β)	$\mathbf{n}_1$	$\mathbf{n}_2$	$\mathbf{k}_{out}$	$\mathbf{P}_{total}$
(0°,0°)	$\begin{pmatrix} 0 \\ 0.7071 \\ 0.7071 \end{pmatrix}$	$\begin{pmatrix} 0 \\ -0.7071 \\ -0.7071 \end{pmatrix}$	$\begin{pmatrix} 0 \\ 0 \\ 1 \end{pmatrix}$	$\begin{pmatrix} 0.9439 - 0.2959i & 0 & 0 \\ 0 & 0.8033 - 0.5584i & 0 \\ 0 & 0 & 1 \end{pmatrix}$
(45°,0°)	$\begin{pmatrix} -0.5 \\ 0.5 \\ 0.7071 \end{pmatrix}$	$\begin{pmatrix} 0.5 \\ -0.5 \\ -0.7071 \end{pmatrix}$	$\begin{pmatrix} 0 \\ 0 \\ 1 \end{pmatrix}$	$\begin{pmatrix} 0.8726 - 0.4271i & 0.0703 + 0.1312i & 0 \\ 0.0703 + 0.1312i & 0.8736 - 0.4271i & 0 \\ 0 & 0 & 1 \end{pmatrix}$
(45°,90°)	$\begin{pmatrix} -0.5 \\ 0.5 \\ 0.7071 \end{pmatrix}$	$\begin{pmatrix} 0 \\ -1 \\ 0 \end{pmatrix}$	$\begin{pmatrix} 0.7071 \\ 0.7071 \\ 0 \end{pmatrix}$	$\begin{pmatrix} 0.5680 - 0.3948i & 0.6247 - 0.3061i & 0 \\ -0.4417 + 0.2164i & 0.4720 - 0.1480i & 0.7071 \\ 0.4417 - 0.216i & -0.4720 + 0.1480i & 0.7071 \end{pmatrix}$
(120°,90°)	$\begin{pmatrix} -0.6124 \\ -0.3536 \\ 0.7071 \end{pmatrix}$	$\begin{pmatrix} 0.9659 \\ -0.2588 \\ 0 \end{pmatrix}$	$\begin{pmatrix} -0.5 \\ 0.8660 \\ 0 \end{pmatrix}$	$\begin{pmatrix} -0.3825 + 0.1874i & 0.6626 - 0.3246i & 0.5 \\ -0.2209 + 0.1082i & 0.3825 - 0.1874i & 0.866 \\ 0.7651 - 0.3749i & 0.4417 - 0.2164i & 0 \end{pmatrix}$
(40°,70°)	$\begin{pmatrix} -0.4545 \\ -0.5417 \\ 0.7071 \end{pmatrix}$	$\begin{pmatrix} -0.0545 \\ -0.9688 \\ -0.2418 \end{pmatrix}$	$\begin{pmatrix} 0.7198 \\ 0.6040 \\ 0.3420 \end{pmatrix}$	$\begin{pmatrix} 0.4473 - 0.2310i & 0.4287 - 0.1727i & 0.7198 \\ -0.6854 + 0.3732i & -0.0621 + 0.0054i & 0.6040 \\ 0.2690 - 0.1728i & -0.7926 + 0.3539i & 0.3420 \end{pmatrix}$
(160°,135°)	$\begin{pmatrix} -0.2418 \\ -0.6645 \\ 0.7071 \end{pmatrix}$	$\begin{pmatrix} 0.7117 \\ 0.4935 \\ 0.5 \end{pmatrix}$	$\begin{pmatrix} -0.6645 \\ 0.2418 \\ -0.7071 \end{pmatrix}$	$\begin{pmatrix} 0.0076 + 0.0835i & -0.6512 + 0.3297i & -0.6645 \\ -0.8342 + 0.4194i & -0.1037 + 0.1634i & 0.2418 \\ -0.2924 + 0.0650i & 0.5765 - 0.2540i & -0.7071 \end{pmatrix}$

Table 2. Diattenuation Associated with Orientation and Ellipticity for Six Groups of Rotation Angles

	$\mathbf{M}_1$			$\mathbf{M}_2$			Total		
Scan Angle (α, β)	D_1	ε_1	θ_1	D_2	ε_2	θ_2	D_{total}	ε_{total}	θ_{total}
(0°,0°)	0.0055	0	0	0.0055	0	0	0.0111	0	0
(45°,0°)	0.0055	0	45	0.0055	0	45	0.0111	0	45
(45°,90°)	0.0055	0	45	0.0055	0	135	0	0	0
(120°,90°)	0.0055	0	120	0.0055	0	30	0	0	0
(40°,70°)	0.0055	0	40	0.0055	0	105.58	0.0038	0.0714	74.89
(160°,135°)	0.0055	0	160	0.0055	0	133.22	0.0078	0.0536	137.67

nearly parallel to each other, and produce a maximum magnitude of diattenuation among these six groups. When $\beta = 90°$, the orientations of diattenuation of the two mirrors are close to orthogonal over the entrance pupil, and the total diattenuation reaches a minimum that is close to zero. The cumulative retardance has similar variations to diattenuation, as shown in Fig. 4.

The polarization aberrations of M1 and M2 are linearly polarized at all the scan angles. However, the ellipticities of total diattenuation and retardance in the last two groups shown in Tables 2 and 3 are not zero. These results indicate that a small amount of circular diattenuation and circular retardance are present, and they can be observed in Figs. 3 and 4 at the rotation angles of (40°,70°) and (160°,135°). Such elliptical diattenuation and elliptical retardance are described in [16], where two linear diattenuators or retarders with axes neither parallel nor perpendicular induce circular polarization.

The periscopic scanner keeps rotating and searching at the pointing, acquisition, and tracking stages [1]. In the range [0°, 360°], the practical rotation angles (α, β) are unpredictable; therefore, the polarization properties should be analyzed considering all possible situations. By varying the rotation angles α and β in the range [0°, 360°] with steps of 1°, the magnitudes of diattenuation and retardance of the periscopic scanner are calculated. Figure 5 shows the variations in cumulative

Table 3. Retardance Associated with Orientation and Ellipticity for Six Groups of Rotation Angles

	$\mathbf{M}_1$			$\mathbf{M}_2$			Total		
Scan Angle (α, β)	δ_1	ε_1	θ_1	δ_2	ε_2	θ_2	δ_{total}	ε_{total}	θ_{total}
(0°,0°)	8.6979	0	90	8.6979	0	90	17.3958	0	90
(45°,0°)	8.6979	0	135	8.6979	0	135	17.3958	0	135
(45°,90°)	8.6979	0	135	8.6979	0	45	0	0	0
(120°,90°)	8.6979	0	30	8.6979	0	120	0	0	0
(40°,70°)	8.6979	0	130	8.6979	0	40	5.9447	0.0356	165
(160°,135°)	8.6979	0	70	8.6979	0	160	12.2949	0.0268	47.5

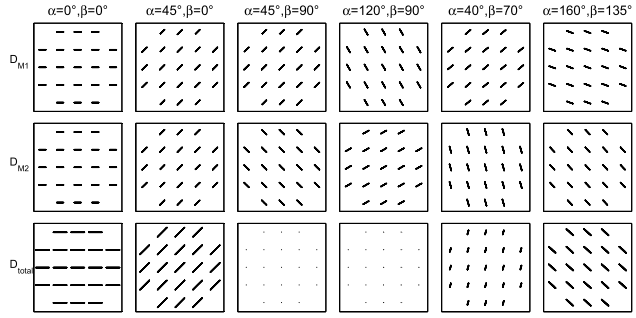

Fig. 3. Diattenuation maps of M1, M2, and the combination of both mirrors for six groups of rotation angles, which are listed in Table 2. The largest diattenuation shown is 0.0111, which occurs at $\beta = 0°$.

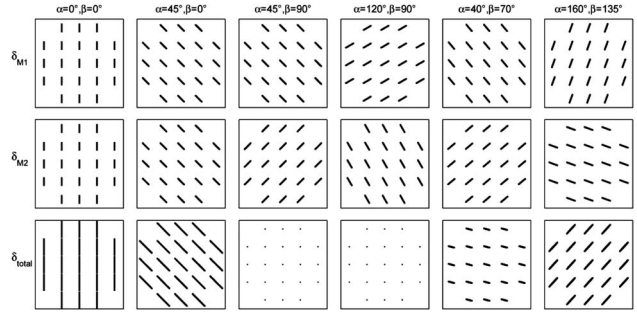

Fig. 4. Retardance maps of M1, M2, and the combination of both mirrors for six groups of rotation angles, which are listed in Table 3. The largest retardance shown is 17.41°, which occurs at $\beta = 0°$.

diattenuation and cumulative retardance for gold-coated mirrors. The units for rotation angle and retardance are degrees.

The amplitudes of diattenuation and retardance vary contiguously and periodically with α and β. The maximum diattenuation and retardance are 0.0111° and 17.41°. The minimum diattenuation and retardance are close to zero. The minimum values indicate that when mirror M2 rotates 90° and 270°, the cumulative diattenuation and retardance of the two mirrors result in cancellation. The polarization effects induced by mirror M1 are completely compensated by the rotation of mirror M2. The periscopic scanner characterizes no polarization aberrations, and the polarization state of the incident beam is unchanged.

5. POLARIZATION PROPERTIES OF THREE DIFFERENT METAL-COATED PERISCOPIC SCANNERS

In this section, three different metal-coated periscopic scanners are created, and the cumulative diattenuation and retardance are analyzed. The output polarization states of the three different scanners are calculated and compared when the input beams are of arbitrary polarization states. These three different metallic coatings are gold, silver, and aluminum. The complex refractive index for gold at 1550 nm is presented in Section 4. Similarly, the complex refractive indices for silver and aluminum are $0.514 + 10.8i$ and $1.440 + 16i$ at the same

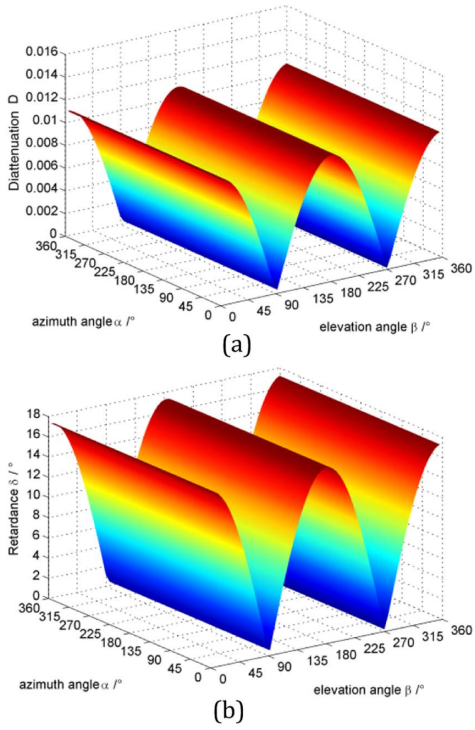

Fig. 5. Cumulative (a) diattenuation and (b) retardance of Au-coated periscopic scanner; the maximum diattenuation and retardance shown are 0.0111 and 17.41°, which occur at $\beta = 0°, 180°, 360°$ scan angles. The minimum diattenuation is close to zero, and the minimum retardance is 0.22°; both minimums occur at $\beta = 90°, 270°$.

wavelength [14,15]. With the periscopic scanners coated with bare metallic films, the complex reflection coefficients for silver at 1550 nm are $r_s = 0.9939\,e^{3.0114i}$, $r_p = 0.9878\,e^{-0.2604i}$; the reflection coefficients for aluminum are $r_s = 0.9922\,e^{3.0541i}$, $r_p = 0.9844\,e^{-0.1750i}$. The calculations of cumulative diattenuation and retardance for silver and aluminum coatings resemble the calculations for gold coatings shown in Section 4. The variations in diattenuation and retardance for silver and aluminum scanners are similar to the diattenuation and retardance shown in Fig. 5, except that the maximum peak values are different. As the rotation of azimuth angle α does not change the magnitudes of diattenuation and retardance, we assume α is a fixed angle, like $\alpha = 0°$. The variations of diattenuation and retardance for the three metal-coated scanners are plotted in Fig. 6 as a function of elevation angle β.

The maxima of diattenuation and retardance occur at $\beta = 0°, 180°, 360°$ scan angles. The maximum diattenuation of the Al-coated scanner is 0.0158, and it is the largest diattenuation compared with the Ag-coated and Au-coated scanners. The maximum diattenuation decreases gradually in the order of aluminum, silver, and gold at the same α and β angles. However, the maximum retardance for aluminum is 10.028°; the value is 14.921° for silver, and the value is 17.407° for gold coatings. The maximum retardance increases gradually in the order of Al, Ag, and Au. The maximum diattenuation and retardance have converse trends of variations. The reason for this phenomenon is the difference in the complex reflection coefficients between *s*- and *p*-polarized light for the three metallic coatings.

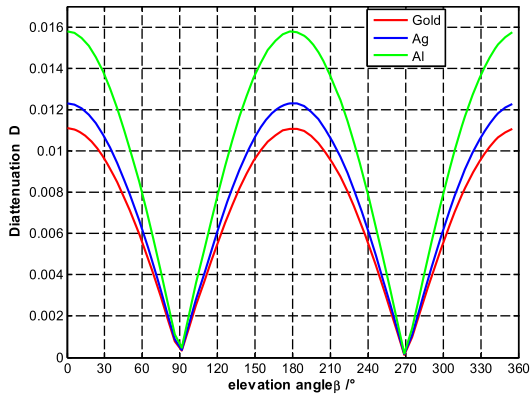

(a)

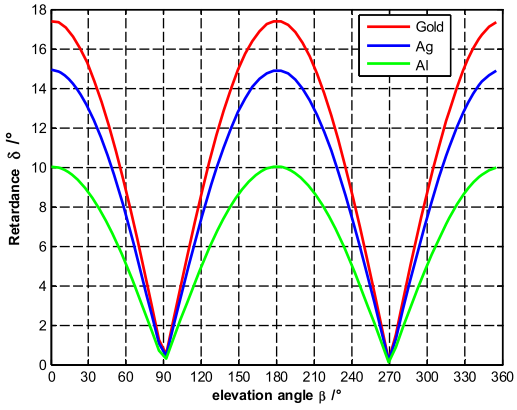

(b)

Fig. 6. (a) Diattenuation and (b) retardance variations for three different metal-coated scanners as a function of elevation angle β with $\alpha = 0°$. Red is for gold coating, blue is for silver coating, and green is for aluminum coating. The minimums of the three curves are close to zero, yet the maximum values are different in (a) and (b).

The diattenuation and retardance affect the input polarization states and reduce the polarization-maintaining capacity of systems. To evaluate the polarization-maintaining capacities of the three different metal-coated scanners, the output polarization states are investigated when the incident beams are of arbitrary polarization states. The three-dimensional Jones vector is expressed as $\mathbf{E}_{\text{in}} = [E_x, E_y, E_z]$. The output polarization is calculated using the vector $\mathbf{E}_{\text{in}}$ and marix $\mathbf{P}_{\text{total}}$ shown in Eq. (15). The output polarization states can be expressed by ellipticity ε and orientation angle θ. Ellipticity ε is the magnitude ratio of the axes of the ellipse, and θ is the orientation of the major axis, measured counterclockwise from the x axis. $\varepsilon = 0$ represents linear polarization, and $\varepsilon = 1$ represents circular polarization. When ε is in the scope of (0, 1), the polarization is elliptical polarization. Positive ε represents right-hand polarization, and negative ε represents left-hand polarization. As the periscopic scanners have even number of mirrors, the output polarization will maintain the input polarization's handedness.

The output polarization states of the periscopic scanners for the three metallic coatings are shown in Figs. 7 and 8. The positions of the polarization state shown in each panel correspond to different pupil positions. Having the same polarization state in each panel means that the polarization aberration

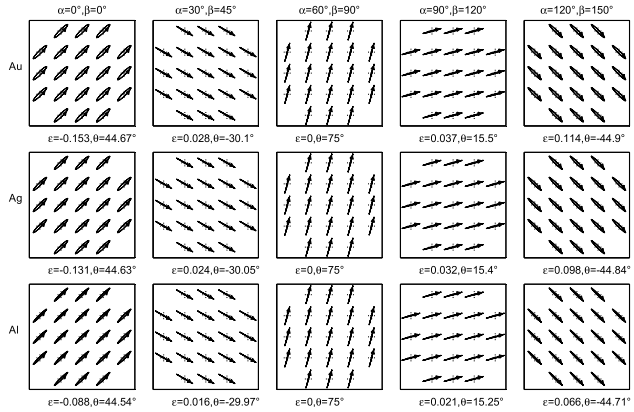

Fig. 7. Output polarization states of three metallic coatings for five groups of rotation angles. The input beams are +45° polarized light. The top row is for the gold-coated scanner, the middle is for the silver-coated scanner, and the last row is for the aluminum-coated scanner. The ellipticity and orientation of the elliptical polarization are given under each panel.

induced by the periscopic scanner remains constant through the whole pupil. Figure 7 shows the azimuth and ellipticity of the output polarization states when the input beams are +45° polarized light, as defined in the initial local coordinates. Figure 8 shows the output polarization states when the input beams are circularly polarized light. The five groups of rotation angles are listed at the top of the panels. The ellipticities ε and orientation angles θ are given below each panel.

The ellipticity ε and orientation θ of the output polarization become functions of the scan angles (α, β). The magnitude of ε represents the shape of the elliptical polarization of the beam. If ε is close to 0, the polarization is close to linear polarization. If the value is close to 1, the polarization is close to circular polarization. As shown in Fig. 7, when the input beam is linearly +45° polarized, the ellipticity of the Al-coated scanner is the smallest one among the three metal-coated scanners at the

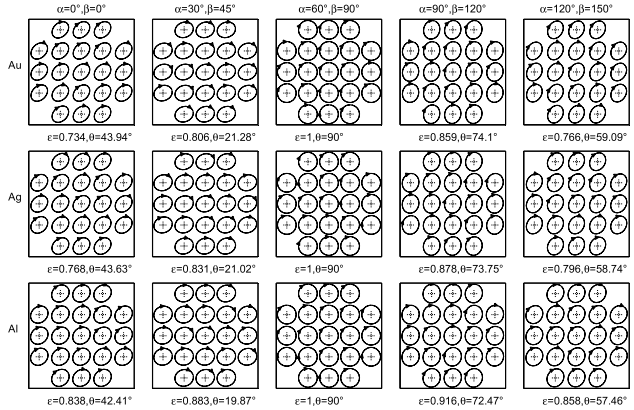

Fig. 8. Output polarization states of the three metallic coatings for five groups of rotation angles. The input beams are right-hand circularly polarized light. The top row is for the gold-coated scanner, the middle is for the silver-coated scanner, and the last row is for the aluminum-coated scanner. The ellipticity and orientation of the elliptical polarization are given under each panel.

same scan angle, which means that the output beam is very close to linear polarization. Similarly, In Fig. 8, when the input beam is right-hand circularly polarized, the ellipticity of the Al-coated scanner is larger than that of the Au-coated and Ag-coated scanners. Therefore, the output elliptical polarization of the Al-coated scanner is closer to circular polarization compared with the Au-coated and Ag-coated scanners. According to Figs. 7 and 8, it is evident that the Al-coated periscopic scanner has a better polarization-maintaining capacity than the Au-coated and Ag-coated scanners.

6. CONCLUSIONS

The optical properties of a two-axis periscopic scanner have been studied in order to understand the polarization properties induced by the scanner. The three-dimensional Jones matrices of the periscopic scanner that maps the initial polarization state into the final polarization state are obtained. For a gold-coated scanner, the variations in diattenuation and retardance are shown as functions of rotation angles α and β. The polarization transformation matrices permit one to predict the output polarization state for any allowed position of a periscopic scanner.

A comparison is performed among three different metal-coated periscopic scanners. The results indicate that the polarization aberrations of the three different metal-coated scanners have similar variations about the scan angles. With an input beam of arbitrary polarization, the output polarization states are calculated and compared among three metal-coated periscopic scanners. The results show that the Al-coated periscopic scanner is a good choice for maintaining polarization.

Funding. National High Technology Research & Development Program of China (2011AA12A103).

REFERENCES

1. K. Böhmer, M. Gregory, F. Heine, H. Kämpfner, and R. Langle, "Laser communication terminals for the European data relay system," Proc. SPIE. **8246**, 82460 (2012).
2. R. A. Chipman, "Polarization analysis of optical systems," Opt. Eng. **28**, 90–99 (1989).
3. R. A. Chipman, "Mechanics of polarization ray tracing," Opt. Eng. **34**, 1636–1645 (1995).
4. J. Sasián, "Polarization fields and wavefronts of two sheets for understanding polarization aberrations in optical imaging systems," Opt. Eng. **53**, 035102 (2014).
5. L. M. Garrison, Z. Blaszczak, and A. E. S. Green, "Polarization characteristics of an azimuth sky scanner," Appl. Opt. **19**, 1419–1424 (1980).
6. C. Beck, R. Schlichenmaier, M. Collados, L. Bellot Rubio, and T. Kentischer, "A polarization model for the German vacuum tower telescope from in situ and laboratory measurements," Astron. Astrophys. **443**, 1047–1053 (2005).
7. G. Anzolin, A. Gardelein, M. Jofre, G. Molina-Terriza, and M. W. Mitchell, "Polarization change induced by a galvanometric optical scanner," J. Opt. Soc. Am. A **27**, 1946–1952 (2010).
8. M. Jofre, G. Anzolin, F. Steinlechner, N. Oliverio, J. P. Torres, V. Pruneri, and M. W. Mitchell, "Fast beam steering with full polarization control using a galvanometric optical scanner and polarization controller," Opt. Express **20**, 12247–12260 (2012).
9. G. Yun, K. Crabtree, and R. A. Chipman, "Three-dimensional polarization ray-tracing calculus I: definition and diattenuation," Appl. Opt. **50**, 2855–2865 (2011).
10. G. Yun, S. C. McClain, and R. A. Chipman, "Three-dimensional polarization ray-tracing calculus II: retardance," Appl. Opt. **50**, 2866–2874 (2011).
11. W. Sze, T. Lam, and R. A. Chipman, "Balancing polarization aberrations in crossed fold mirrors," Appl. Opt. **54**, 3236–3245 (2015).
12. E. Waluschka, "Polarization ray trace," Opt. Eng. **28**, 280286 (1989).
13. R. A. Chipman, "Muller matrices," in *Handbook of Optics*, Vol. **I** of Geometrical and Physical Optics, Polarized Light, Components and Instruments (McGraw-Hill, 2010), Chap. 14.
14. E. D. Palik, *Handbook of Optical Constants of Solids* (Academic, 1991).
15. Flilmetrics, http://www.filmetrics.com/refractive-index-database.
16. D. B. Chenault and R. A. Chipman, "Measurements of linear diattenuation and linear retardance spectra with a rotating sample spectropolarimeter," Appl. Opt. **32**, 3513–3519 (1993).